Inorganic Chemistry
Article

Inorg. Chem. **2009**, *48*, 11853–11864 **11853**
DOI: 10.1021/ic901900g

The Semiquinone−Ruthenium Combination as a Remarkably Invariant Feature in the Redox and Substitution Series $[Ru(Q)_n(acac)_{3-n}]^m$, $n = 1-3$; $m = (-2), -1, 0, +1, (+2)$; Q = 4,6-Di-*tert*-butyl-*N*-phenyl-*o*-iminobenzoquinone

Dipanwita Das,[†] Atanu Kumar Das,[‡] Biprajit Sarkar,[‡] Tapan Kumar Mondal,[⊥] Shaikh M. Mobin,[†] Jan Fiedler,[§] Stanislav Záliš,[§] Francisco A. Urbanos,[∥] Reyes Jiménez-Aparicio,*[,⊥] Wolfgang Kaim,*[,‡] and Goutam Kumar Lahiri*[,†]

[†]*Department of Chemistry, Indian Institute of Technology Bombay, Powai, Mumbai-400076, India,* [‡]*Institut für Anorganische Chemie, Universität Stuttgart, Pfaffenwaldring 55, D-70550 Stuttgart, Germany,* [§]*J. Heyrovský Institute of Physical Chemistry, v.v.i., Academy of Sciences of the Czech Republic, Dolejškova 3, CZ-18223 Prague, Czech Republic,* [∥]*Departamento de Química Inorgánica, Facultad de Ciencias Químicas, Universidad Complutense, Ciudad Universitaria, E-28040 Madrid, Spain, and* [⊥]*Department of Chemistry, Jadavpur University, Jadavpur, Kolkata-700032, India*

Received September 26, 2009

Three new compounds, $[Ru(Q^{\bullet-})(acac)_2]$ = **1**, $[Ru(Q^{\bullet-})_2(acac)]$ = **2**, and $[Ru(Q^{\bullet-})_3]$ = **3**, were obtained and characterized as Ru^{III} complexes with 4,6-di-*tert*-butyl-N-phenyl-*o*-iminobenzosemiquinone ($Q^{\bullet-}$) ligands. All three systems show multiple electron transfer behavior, which was analyzed using electron paramagnetic resonance (EPR) and UV−vis−near-infrared (NIR) spectroelectrochemistry. ^{1}H NMR spectroscopy and a crystal structure analysis suggest antiferromagnetically spin−spin coupled Ru^{III} and $Q^{\bullet-}$ in **1**, similar to that in the related compound **4** with unsubstituted *o*-iminobenzosemiquinone. However, in contrast to $\mathbf{4}^n$ (Remenyi, C.; Kaupp, M. *J. Am. Chem. Soc.* **2005**, *127*, 11399), the system $\mathbf{1}^m$ exhibits unambiguously metal-centered electron transfer, producing ions $[Ru^{IV}(Q^{\bullet-})(acac)_2]^+ = \mathbf{1}^+$ and $[Ru^{II}(Q^{\bullet-})(acac)_2]^- = \mathbf{1}^-$, both with EPR-evidenced ligand-based spin, as also supported by DFT calculations. Compared with the related redox system $[Ru(Q)(bpy)_2]^k$ ($\mathbf{5}^k$) ($k = 0-3$), the spectroelectrochemical similarity suggests corresponding electronic structures except for the $\mathbf{1}^+/\mathbf{5}^{3+}$ pair ($[Ru^{IV}(Q^{\bullet-})(acac)_2]^+$ ($\mathbf{1}^+$) versus $[Ru^{III}(Q^0)(bpy)_2]^{3+}$ ($\mathbf{5}^{3+}$)). Compound **2**, a three-spin system $[Ru^{III}(Q^{\bullet-})_2(acac)]$ obtained in the all-cis configuration, possesses a complicated magnetic behavior including strong intramolecular antiferromagnetic coupling (J_{Ru-Q}, on the order of -10^3 cm^{-1} and J_{Q-Q}, -10^2 cm^{-1}) and weak intermolecular antiferromagnetic and ferromagnetic interactions. Strong intramolecular coupling leads to one unpaired electron at low temperatures, as also supported by the radical-type EPR signal of the solid and of solutions, which diminishes at higher temperatures. The up−down−up spin arrangement for the ground state of $\{(Q^{\bullet-})-Ru^{III}-(Q^{\bullet-})\}$ ($S = 1/2$) is confirmed by DFT calculations for **2**. Oxidation to $\mathbf{2}^+$ leaves the UV−vis−NIR spectrum almost unchanged, whereas reduction to $\mathbf{2}^-$ and $\mathbf{2}^{2-}$ produces low-energy absorptions. The ligand-centered spin for $\mathbf{2}^{2-} = [Ru^{II}(Q^{\bullet-})(Q^{2-})(acac)]^{2-}$ suggests the $[Ru^{II}(Q^{\bullet-})_2(acac)]^-$ formulation for $\mathbf{2}^-$. Compound **3**, obtained as a structurally characterized mer isomer, has a predominantly ligand-centered highest occupied molecular orbital (HOMO), as evident from the EPR signal of the intermediate $\mathbf{3}^+$ and as supported by DFT calculations. In contrast, electron addition proceeds to yield a metal/ligand mixed spin intermediate $\mathbf{3}^-$ according to EPR, in agreement with ca. 25% calculated metal character of the lowest unoccupied molecular orbital (LUMO). The near-infrared absorption of **3** at 1280 nm corresponds to the HOMO−LUMO transition (ligand-to-metal/ligand-to-ligand charge transfer). Oxidation to $\mathbf{3}^+$ produces a weak broad band at about 2500 nm, while the reduction to $\mathbf{3}^-$ gives rise to an intense absorption feature at 816 nm. The valence state alternatives are being discussed for all spectroelectrochemically accessible species, and the individual results are compared across this unique substitution and redox series involving a highly noninnocent ligand/metal combination. All established oxidation state formulations involve the iminosemiquinone−ruthenium entity, illustrating the remarkable stability of that arrangement, which corroborates the use of this combination in water oxidation catalysis.

Introduction

The combination between redox-active ruthenium and non-innocent[1] bidentate ligands of the *o*-quinone (1,2-dioxolene) type has led to a fascinating array of compounds. The intricate intramolecular charge, spin, and electron transfer phenomena result in highly variable valence configurations and often reflect considerable ligand−metal orbital mixing (covalency).[2−6] Herein, we can present for the first time a complete substitution series $[Ru(Q)_n(acac)_{3-n}]^m$, $n = 1-3$,

*To whom correspondence should be addressed. E-mail: lahiri@chem.iitb.ac.in (G.K.L.), kaim@iac.uni-stuttgart.de (W.K.).

© 2009 American Chemical Society
Published on Web 11/24/2009

with charges m ranging from −2 (for some species) via −1, 0, and +1, up to +2 in some instances. Q is the well-applied and recently reviewed 4,6-di-*tert*-butyl-*N*-phenyl-*o*-iminobenzoquinone,[7] which was shown to form persistent transition metal compounds in all three oxidation states, Q^o, $Q^{\bullet -}$, and Q^{2-}. The ruthenium compounds were isolated and initially characterized as the neutral species, while their oxidized and reduced forms were studied by cyclic voltammetry, electron paramagnetic resonance (EPR), and UV−vis−near-infrared (NIR) spectroelectrochemistry. Compounds $\mathbf{1}^m$, $\mathbf{2}^m$, and $\mathbf{3}^m$ were subjected to density functional theory (DFT) and time-dependent density functional theory (TD-DFT) calculations to interpret the experimental data and establish the electronic structures. While compounds **1**−**3** are new, the NH analog $\mathbf{4}^n$[8] of the NPh system $\mathbf{1}^m$ and the species $[Ru(Q)(bpy)_2]^k$ ($\mathbf{5}^k$), k = 0−3[6] have been reported. Within the series $[Ru(Q)_n(acac)_{3-n}]^m$, the n = 0 parent species, $Ru(acac)_3$ (**6**),[9,10] is a long-known compound. Of the related compounds, $[Ru(L)(acac)_2]$, the derivative with L = diimino-*o*-benzoquinone has been extensively studied and reported recently,[2i] while the L = *o*-benzoquinone series will be presented by us in a separate report.

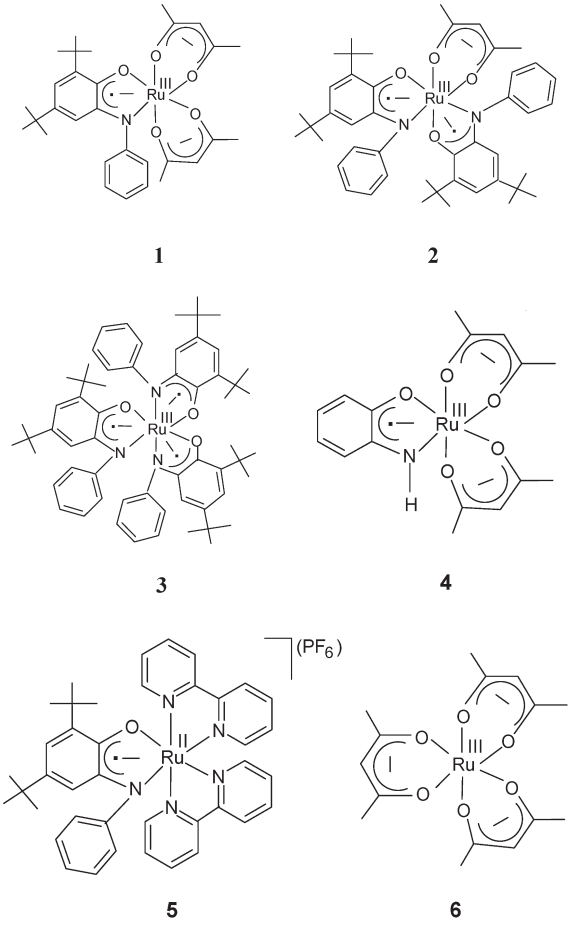

Results and Discussion

Synthesis and Basic Characterization of Neutral Compounds. The diamagnetic $[Ru(Q^{\bullet -})(acac)_2]$ (**1**) and paramagnetic $[Ru(Q^{\bullet -})_2(acac)]$ (**2**) ($acac^-$ = 2,4-pentanedionato, $Q^{\bullet -}$ = iminobenzosemiquinone) have been obtained from the reaction of $Ru^{II}(acac)_2(CH_3CN)_2$ with 2-anilino-4,6-di-*tert*-butyl-phenol (H_2Q) in refluxing ethanol and in the presence of a sodium acetate base under aerobic conditions, followed by chromatographic separation using a silica gel column. The complex $[Ru(Q^{\bullet -})_3]$ (**3**) has been synthesized by the reaction of $RuCl_3$ with H_2Q in methanol in the presence of KOH under atmospheric conditions, followed by chromatographic purification (see the Experimental Section).

The neutral complexes **1**, **2** in CH_3CN, and **3** in CH_2Cl_2 exhibit molecular ion peaks at m/z = 596.35, 791.52, and 987.47, respectively, corresponding to $\mathbf{1}^+$ (calculated mass = 595.19), $\mathbf{2}^+$ (calculated mass = 791.33), and $\mathbf{3}^+$ (calculated mass = 987.48) and give satisfactory microanalytical data (Experimental Section).

(1) "Non-innocent" ligands can occur in at least two readily accessible oxidation states, which may introduce ambiguity in oxidation state assignment unless the "correct" oxidation numbers for the metal and ligand can be proven experimentally. (a) Jørgensen, C. K. *Coord. Chem. Rev.* **1966**, *1*, 164. (b) Ward, M. D.; McCleverty, J. A. *J. Chem. Soc., Dalton Trans.* **2002**, 275. (c) Herebian, D.; Bothe, E.; Bill, E.; Weyhermüller, T.; Wieghardt, K. *J. Am. Chem. Soc.* **2001**, *123*, 10012.

(2) (a) Haga, M.; Dodsworth, E. S.; Lever, A. B. P. *Inorg. Chem.* **1986**, *25*, 447. (b) Masui, H.; Lever, A. B. P.; Auburn, P. *Inorg. Chem.* **1991**, *30*, 2402. (c) Ebadi, M.; Lever, A. B. P. *Inorg. Chem.* **1999**, *38*, 467. (d) Lever, A. B. P.; Auburn, P. R.; Dodsworth, E. S.; Haga, M.; Liu, W.; Melnik, M .; Nevin, W. A. *J. Am. Chem. Soc.* **1988**, *110*, 8076. (e) Auburn, P. R.; Dodsworth, E. S.; Haga, M.; Liu, W.; Nevin, W. A.; Lever, A. B. P. *Inorg. Chem.* **1991**, *30*, 3502. (f) Lever, A. B. P.; Gorelsky, S. L. *Struct. Bonding* (*Berlin*) **2004**, *107*, 77. (g) Haga, M.; Dodsworth, E. S.; Lever, A. B. P.; Boone, S. R.; Pierpont, C. G. *J. Am. Chem. Soc.* **1986**, *108*, 7413. (h) Meacham, A. P.; Druce, K. L.; Bell, Z. R.; Ward, M. D.; Keister, J. B.; Lever, A. B. P. *Inorg. Chem.* **2003**, *42*, 7887. (i) Kalinina, D.; Dares, D.; Kaluarachchi, H.; Potvin, P. G.; Lever, A. B. P. *Inorg. Chem.* **2008**, *47*, 10110.

(3) (a) Pierpont, C. G. *Coord. Chem. Rev.* **2001**, *219*−*221*, 415. (b) Bhattacharya, S.; Boone, S. R.; Fox, G. A.; Pierpont, C. G. *J. Am. Chem. Soc.* **1990**, *112*, 1088. (c) Bhattacharya, S.; Pierpont, C. G. *Inorg. Chem.* **1991**, *30*, 1511. (d) Boone, S. R.; Pierpont, C. G. *Inorg. Chem.* **1987**, *26*, 1769. (e) Bhattacharya, S.; Pierpont, C. G. *Inorg. Chem.* **1994**, *33*, 6038. (f) Pierpont, C. G.; Lange, C. W. *Prog. Inorg. Chem.* **1994**, *41*, 331. (g) Pierpont, C. G.; Attia, A. S. *Collect. Czech. Chem. Commun.* **2001**, *66*, 33.

(4) (a) Ernst, S.; Kasack, V.; Bessenbacher, C.; Kaim, W. *Z. Naturforsch.* **1987**, *42b*, 425. (b) Kasack, V.; Kaim, W.; Binder, H.; Jordanov, J.; Roth, E. *Inorg. Chem.* **1995**, *34*, 1924. (c) Knödler, A.; Fiedler, J.; Kaim, W. *Polyhedron* **2004**, *23*, 701. (d) Ernst, S.; Hänel, P.; Jordanov, J.; Kaim, W.; Kasack, V.; Roth, E. *J. Am. Chem. Soc.* **1989**, *111*, 1733. (e) Kaim, W.; Wanner, M.; Knödler, A.; Záliš, S. *Inorg. Chim. Acta* **2002**, *337*, 163.

(5) (a) Bag, N.; Pramanik, A.; Lahiri, G. K.; Chakravorty, A. *Inorg. Chem.* **1992**, *31*, 40. (b) Bag, N.; Lahiri, G. K.; Basu, P.; Chakravorty, A. *J. Chem. Soc., Dalton Trans.* **1992**, 113. (c) Okamura, R.; Wada, T.; Aikawa, K.; Nagata, T.; Tanaka, K. *Inorg. Chem.* **2004**, *43*, 7210. (d) Cheng, H.-Y.; Lin, C.-C.; Tzeng, B.-C.; Peng, S.-M. *J. Chin. Chem. Soc.* **1994**, *41*, 775. (e) Mitra, K. N.; Majumder, P.; Peng, S.-M.; Castinẽiras, A.; Goswami, S. *Chem.Commun.* **1997**, 1267. (f) Mitra, K. N.; Choudhury, S.; Castinẽiras, A.; Goswami, S. *J. Chem. Soc., Dalton Trans.* **1998**, 2901. (g) Das, C.; Kamar, K. K.; Ghosh, A. K.; Mjumdar, P.; Hung, C.-H.; Goswami, S. *New J. Chem.* **2002**, *26*, 1409. (h) Connelly, N. G.; Manners, I.; Protheroe, J. R. C.; Whiteley, M. W. *J. Chem. Soc., Dalton Trans.* **1984**, 2713. (i) Kurihara, M.; Daniele, S.; Tsuge, K.; Sugimoto, H.; Tanaka, K. *Bull. Chem. Soc. Jpn.* **1998**, *71*, 867. (j) Salmonsen, R. B.; Abelleira, A.; Clarke, M. J. *Inorg. Chem.* **1984**, *23*, 387. (k) Dei, A.; Gatteschi, D.; Pardi, L. *Inorg. Chem.* **1990**, *29*, 1443. (l) Patra, S.; Sarkar, B.; Ghumaan, S.; Fiedler, J.; Zalis, S.; Kaim, W.; Lahiri, G. K. *J. Chem. Soc., Dalton Trans.* **2004**, 750. (m) Maji, S.; Patra, S.; Chakraborty, S.; Mobin, S. M.; Janardanan, D.; Sunoj, R. B.; Lahiri, G. K. *Eur. J. Inorg. Chem.* **2007**, 314. (n) Das, D.; Mondal, T. K.; Mobin, S. M.; Lahiri, G. K. *Inorg. Chem.* **2009**, *48*, 9800.

(6) Ye, S.; Sarkar, B.; Duboc, C.; Fiedler, J.; Kaim, W. *Inorg. Chem.* **2005**, *44*, 2843.

(7) Poddelsky, A. I.; Cherkasov, V. V.; Abakumov, G. A. *Coord. Chem. Rev.* **2009**, *253*, 291.

(8) Patra, S.; Sarkar, B.; Mobin, S. M.; Kaim, W.; Lahiri, G. K. *Inorg. Chem.* **2003**, *42*, 6469.

(9) Endo, A.; Watanabe, M.; Hayashi, S.; Shimizu, K.; Sato, G. P. *Bull. Chem. Soc. Jpn.* **1978**, *51*, 800.

(10) Johnson, A.; Everett, G. W. *J. Am. Chem. Soc.* **1972**, *94*, 1419.

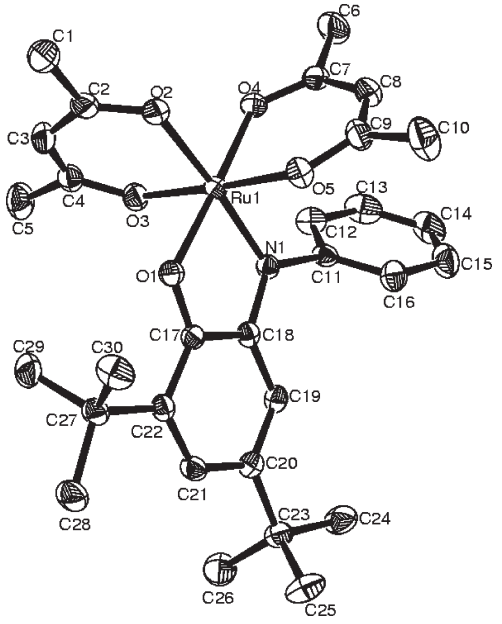

Figure 1. ORTEP diagram of **1**. Ellipsoids are drawn at 50% probability.

Table 1. Selected Crystallographic Data for **1** and **3**

	1	**3**
mol formula	$C_{30}H_{39}NO_5Ru$	$C_{60}H_{75}N_3O_3Ru$
fw	594.71	987.35
cryst sym	triclinic	orthorhombic
space group	$P\bar{1}$	$P2_12_12_1$
a (Å)	8.8841(10)	13.130(8)
b (Å)	11.9536(7)	17.425(9)
c (Å)	14.2928(7)	23.345(11)
α (deg)	88.701(4)	90
β (deg)	80.169(6)	90
γ (deg)	79.386(7)	90
V (Å^3)	1469.9(2)	5341(5)
Z	2	4
μ (mm^{-1})	0.570	0.339
T (K)	150(2)	150(2)
D_{calcd} (g cm^{-3})	1.344	1.228
F (000)	620	2096
2θ range (deg)	3.18 to 25.00	2.94 to 25.00
data/restraints/params	5168/0/344	9383/0/622
R1, wR2 [$I > 2\sigma(I)$]	0.0277, 0.0691	0.0465,0.0425
R1, wR2 (all data)	0.0318, 0.0699	0.1724, 0.0608
GOF	1.133	0.507
largest diff. peak/hole, (e Å^{-3})	0.461 and −0.297	0.366 and −0.477

All three compounds **1**−**3** can exist as isomers. While compound **1** can only form a pair of enantiomers (Figure 1, Tables 1 and 2), there are three positional isomers possible for a case such as **2**: all-*cis* (*ccc*), O-*trans* (*ctc*), or N-*trans* (*cct*).[11,12] Since the very soluble paramagnetic compound **2**, isolated as a single isomer species via chromatography, could not be crystallized for X-ray diffraction, IR spectroscopy was used to investigate the configuration. While both the free ligand H_2Q and complex **1** show a single vibrational band at 2961 cm^{-1}, the isolated isomer of **2** displays two such absorption features at 2960 and 2923 cm^{-1}. We therefore assume the *ccc* (all-*cis*) form to be present, which is the only isomer with nonequivalent N-phenyl positions. In addition, steric

Table 2. Selected Bond Distances (Å) for **1**

bond distances	exptl	calcd
Ru(1)−O(1)	1.9897(18)	2.037
Ru(1)−O(2)	2.0364(18)	2.029
Ru(1)−O(3)	2.0070(19)	2.054
Ru(1)−O(4)	2.0395(18)	2.053
Ru(1)−O(5)	2.0274(19)	2.028
Ru(1)−N(1)	1.937(2)	1.953
C(2)−O(2)	1.267(3)	1.286
C(4)−O(3)	1.278(3)	1.284
C(7)−O(4)	1.261(3)	1.286
C(9)−O(5)	1.280(3)	1.289
C(17)−O(1)	1.291(3)	1.316
C(18)−N(1)	1.354(3)	1.365
C(17)−C(18)	1.427(4)	1.457
C(18)−C(19)	1.416(4)	1.434
C(19)−C(20)	1.363(4)	1.386
C(20)−C(21)	1.429(4)	1.437
C(21)−C(22)	1.359(4)	1.386
C(22)−C(17)	1.429 (4)	1.428

factors also favor the *ccc* configuration since the *ctc* and *cct* isomers suffer from steric constraints due to the presence of two close N-phenyl rings or ^{t}Bu groups. System **3** can exist in facial and meridional diastereoisomeric forms. However, the three observed IR bands at 2952, 2903, and 2863 cm^{-1} and the ^{1}H NMR resonances (see below) of the isolated isomer clearly establish the mer form of **3**. The mer structure of **3** has also been authenticated by its single-crystal X-ray structure (Tables 1 and 3, Figure 2). Analogous tris complexes of cobalt(III) and iron(III) were also reported in meridional form.[13]

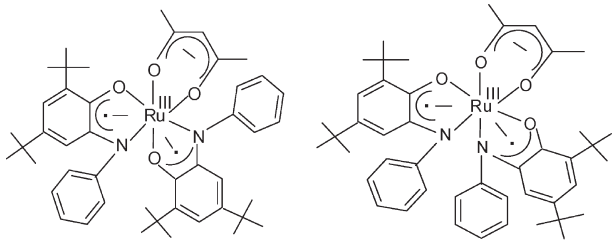

2-*ccc* **2-*ctc* (O-*trans*)**

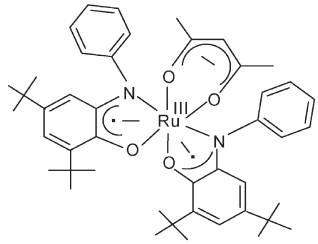

2-*cct* (N-*trans*)

The diamagnetic **1** exhibits the calculated number of partially overlapping signals from seven different "aromatic" protons between 7.1 and 7.4 ppm in addition to well-resolved "aliphatic" proton signals, two CH(acac)'s at 5.14/5.62, four CH_3(acac)'s at 2.62/2.0/1.99/1.82, and two ^{t}Bu signals at 1.56/1.45 ppm. The ^{1}H NMR spectrum of **3**

(11) Krause, R. A.; Krause, K. *Inorg. Chem.* **1980**, *19*, 2600.
(12) Patra, S.; Sarkar, B.; Ghumaan, S.; Patil, M. P.; Mobin, S. M.; Sunoj, R. B.; Kaim, W.; Lahiri, G. K. *Dalton Trans.* **2005**, 1188.
(13) (a) Chaudhuri, P.; Wagner, R.; Pieper, U.; Biswas, B.; Weyhermüller, T. *Dalton Trans.* **2008**, 1286. (b) Mukherjee, S.; Weyhermüller, T.; Bill, E.; Wieghardt, K.; Chaudhuri, P. *Inorg. Chem.* **2005**, *44*, 7099.

Table 3. Selected Bond Distances (Å) for **3**

bond distances	exptl	calcd
Ru(1)−O(1)	2.019(4)	2.021
Ru(1)−O(2)	2.019(4)	2.021
Ru(1)−O(3)	1.982(5)	2.021
Ru(1)−N(1)	2.006(6)	1.988
Ru(1)−N(2)	1.958(6)	1.988
Ru(1)−N(3)	1.993(7)	1.988
C(1)−O(1)	1.316(8)	1.297
C(6)−N(1)	1.325(8)	1.358
C(21)−O(2)	1.309(7)	1.297
C(26)−N(2)	1.377(9)	1.358
C(41)−O(3)	1.336(8)	1.297
C(46)−N(3)	1.364(9)	1.358
C(1)−C(2)	1.431(10)	1.413
C(2)−C(3)	1.385(9)	1.378
C(3)−C(4)	1.437(9)	1.405
C(4)−C(5)	1.360(9)	1.379
C(5)−C(6)	1.413(9)	1.411
C(6)−C(1)	1.379(10)	1.441
C(21)−C(22)	1.416(9)	1.413
C(22)−C(23)	1.406(8)	1.378
C(23)−C(24)	1.403(9)	1.405
C(24)−C(25)	1.358(9)	1.379
C(25)−C(26)	1.438(8)	1.411
C(26)−C(21)	1.411(9)	1.441
C(41)−C(42)	1.398(10)	1.413
C(42)−C(43)	1.398(8)	1.378
C(43)−C(44)	1.415(10)	1.405
C(44)−C(45)	1.365(10)	1.379
C(45)−C(46)	1.443(8)	1.411
C(46)−C(41)	1.423(10)	1.441

exhibits partially overlapping signals for 21 "aromatic" protons in the range of 7.15−5.95 ppm; three distinct ^{t}Bu signals at 1.11, 0.98, and 0.91 ppm; and three more ^{t}Bu resonances overlapping between 1.21 and 1.15 ppm. The appearance of six distinct ^{t}Bu signals and three sets each of 2H and 5H aromatic protons corresponding to three magnetically nonequivalent Q ligands indicates a C_1 symmetric meridional configuration of **3** in solution.[14]

The diffraction data of **1** and **3** (Tables 1−3, Figures 1 and 2) suggest the Ru^{III}−iminosemiquinone formulation. According to established correlations,[13,15,16] the intermediate values for C−O bond lengths (1.291(3) Å for **1** and 1.320 (av) Å for **3**, 1.316 and 1.297 Å from DFT), C−N bond distances (1.354(3) Å for **1** and 1.355 (av) Å for **3**, 1.365 and 1.358 Å from DFT), and C−C(meta) bond lengths (1.361 (av) for **1** and 1.379 (av) for **3**, 1.386 and 1.378 Å from DFT) indicate the semiquinone state of the ligand. The C−C(meta) distances, for example, C(19)−C(20) and C(21)−C(22), are most indicative[15,16g] because they show the transition from an aromatic C−C bond (bond order 1.5, ca. 1.39 Å) to a double bond in a quinone-type structure (ca. 1.34 Å). All available geometrical parameters are reproduced by the calculated bond values as obtained from DFT-optimized structures (Tables 2 and 3 and and Table S1, Supporting Information).

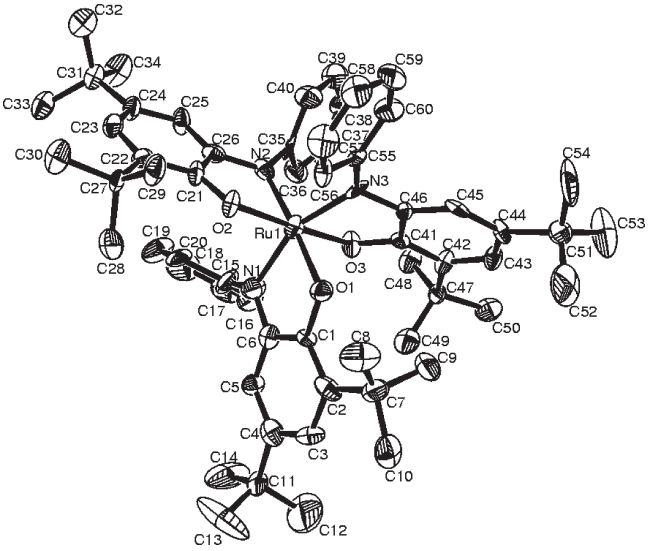

Figure 2. ORTEP diagram of **3**. Ellipsoids are drawn at 50% probability.

The Three-Spin Exchange Compound 2: Temperature-Dependent Susceptibility and EPR. As an odd electron species, the neutral compound **2** is expected to exhibit an EPR response. However, the complex is EPR-silent at room temperature; on lowering the temperature, a radical-type EPR signal is observed in solution (g = 1.99) and in the solid (g = 1.98) **2** (Figure 3). The alternative, an EPR signal with widely spread **g** tensor components ($2.9 > g_x > 1.2$), as would be expected for ruthenium-centered spin like in well-studied[17] $Ru(acac)_3$ (**6**: low-spin $4d^5$ configuration), is not observed. The spin density representation of the three-spin complex **2** (0.720, 0.268, and 0.011 for Q, Ru, and acac, respectively; Figures S1 and S2 (optimized structure of **2**) and Table S2, Supporting Information) also reveals that the antiferromagnetic coupling between one $Q^{\bullet-}$ and Ru^{III} leaves the remaining unpaired spin on the second $Q^{\bullet-}$ site, representing an up−down−up spin alignment.

Ligand-centered spin but diminishing EPR intensity at higher temperatures would be in agreement with a three-spin exchange coupling situation involving two noncoplanar iminosemiquinone radicals interacting with the central (S = 1/2) metal ion. Such a situation has been found recently for a copper(II) compound, **7**, containing two modified 4,6-di-*tert*-butyl-N-aryl-*o*-iminobenzosemiquinone ligands.[18] Weak interligand exchange due to non-coplanarity in **7** favors an up−down−up spin alignment as the ground state, in contrast to the up−up−down situation with strong antiferromagnetic

(14) Tamayo, A. B.; Alleyne, B. D.; Djurovich, P. I.; Lamansky, S.; Tsyba, I.; Ho, N. N.; Bau, R.; Thompson, M. E. *J. Am. Chem. Soc.* **2003**, *125*, 7377.

(15) Bhattacharya, S.; Gupta, P.; Basuli, F.; Pierpont, C. G. *Inorg. Chem.* **2002**, *41*, 5810.

(16) (a) Verani, C. N.; Gallert, S.; Bill, E.; Weyhermüller, T.; Wieghardt, K.; Chaudhuri, P. *Chem. Commun.* **1999**, 1747. (b) Chun, H.; Verani, C. N.; Chaudhuri, P.; Bothe, E.; Bill, E.; Weyhermüller, T.; Wieghardt, K. *Inorg. Chem.* **2001**, *40*, 4157. (c) Chun, H.; Chaudhuri, P.; Weyhermüller, T.; Wieghardt, K. *Inorg. Chem.* **2002**, *41*, 790. (d) Sun, X.; Chun, H.; Hildenbrand, K.; Bothe, E.; Weyhermüller, T.; Neese, F.; Wieghardt, K. *Inorg. Chem.* **2002**, *41*, 4295. (e) Chun, H.; Weyhermüller, T.; Bill, E.; Wieghardt, K. *Angew. Chem., Int. Ed.* **2001**, *40*, 2489. (f) Roy, N.; Sproules, S.; Weyhermüller, T.; Wieghardt, K. *Inorg. Chem.* **2009**, *48*, 3783. (g) Samanta, S.; Singh, P.; Fiedler, J.; Zalis, S.; Kaim, W.; Goswami, S. *Inorg. Chem.* **2008**, *47*, 1625. (h) Chatterjee, S.; Singh, P.; Fiedler, J.; Bakova, R.; Zalis, S.; Kaim, W.; Goswami, S. *Dalton Trans.* **2009**, 7778.

(17) (a) DeSimone, R. E. *J. Am. Chem. Soc.* **1973**, *95*, 6238. (b) Reynolds, P. A.; Cable, J. W.; Sobolev, A. N.; Figgis, B. N. *J. Chem. Soc., Dalton Trans.* **1998**, 559. (c) Jarrett, H. S. *J. Chem. Phys.* **1957**, *27*, 1298. (d) Saha, M. *Indian J. Phys.* **1969**, *43*, 646.

(18) Ye, S.; Sarkar, B.; Lissner, F.; Scheid, T.; Slageren, J. V.; Fiedler, J.; Kaim, W. *Angew. Chem., Int. Ed.* **2005**, *44*, 2103.

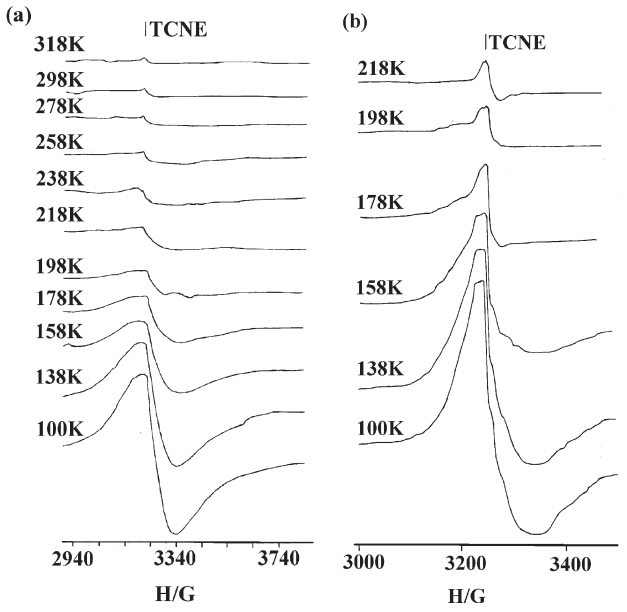

Figure 3. EPR spectra of **2**: (a) solid and (b) in CH_3CN solution at variable temperatures. The *g* value of the TCNE standard is 2.00273.

ligand−ligand interaction invoked for the coplanar analog $[Cu^{II}(Q^{\bullet-})_2]$ (**8**).[19]

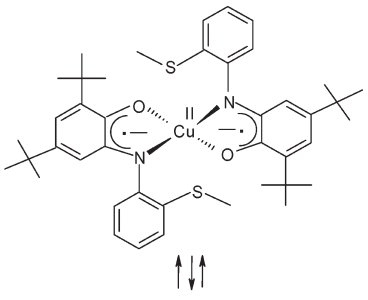

7

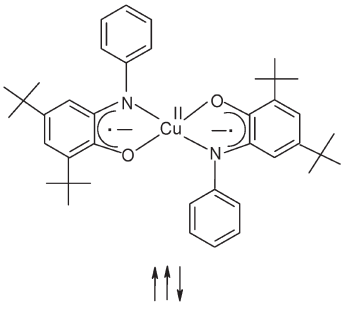

8

The magnetic susceptibility of **2** between 300 and 2 K has been measured at different magnetic fields. In all cases, the magnetic susceptibility increases with decreasing temperature. However, the susceptibility values vary with the magnetic field, and the dependence of the magnetic moment is especially marked (Figure 4 and Figures S3−S5, Supporting Information). The magnetic

(19) Chaudhuri, P.; Verani, C. N.; Bill, E.; Bothe, E.; Weyhermüeller, T.; Wieghardt, K. *J. Am. Chem. Soc.* **2001**, *123*, 2213.

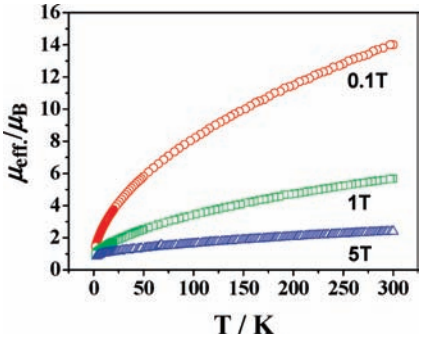

Figure 4. Temperature dependence of magnetic moment under magnetic fields of 0.1 (○, red), 1 (□, green), and 5 (△, blue) T of **2**.

moment at room temperature is 14.00, 5.68, and 2.40 μ_B at 0.1, 1, and 5 T, respectively. Under all measured magnetic fields, the magnetic moments decrease with temperature and converge to ~1 μ_B. Thus, the magnetic moment value at 2 K is slightly lower than that expected for an $S = 1/2$ spin system, which is in accordance with the EPR results at low temperatures (Figure 3).

The variation of the magnetic susceptibility and the magnetic moment under different magnetic fields clearly indicates the presence of ferromagnetism in this compound, especially at room temperature. However, the strong decrease of the magnetic moment with the temperature indicates the coexistence of a predominant antiferromagnetic interaction.

Magnetization measurements at 300, 100, and 2 K have been carried out (Figure S6 and Figure S7, Supporting Information). In all cases, the representation of the magnetization toward magnetic field is not linear. The most noticeable of these data is the saturation of the magnetization at 300 K at ca. 1 T. In contrast, the saturation at 2 K is not reached (Figure S6).

The saturation of the magnetization at 300 K, and also the slope of the curve at 100 K, confirms the presence of ferromagnetic interactions at higher temperatures. However, the spin value calculated from the molar magnetization at saturation is 0.01, too low even for the existence of only one unpaired electron. Small hysteresis loops are observed at 300 and 2 K (Figures S8 and S9, Supporting Information), which confirm unequivocally the presence of a ferromagnetic component in the entire range of the measured temperatures.

The zero-field-cooled (ZFC) and field-cooled (FC) thermomagnetization curves at a low magnetic field (0.1 T) exhibit irreversibility from 300 K, which also confirms the existence of ferromagnetic order just below this temperature (Figure S10, Supporting Information).

We have carried out magnetization measurements at 5 T in order to saturate the ferromagnetic effect. As one can see in Figure 4 and Figures S3−S5, at this field, the room-temperature magnetic moment is 2.40 μ_B, lower than that expected for three unpaired electrons per molecule (3.87 μ_B), which suggests dominant strong intramolecular antiferromagnetic contacts under these conditions. The decrease of the magnetic moment with decreasing temperature confirms this antiferromagnetic coupling. In addition, an intermolecular antiferromagnetic interaction must also exist because the magnetic moment (1 μ_B) at 2 K is lower than that expected for one unpaired electron.

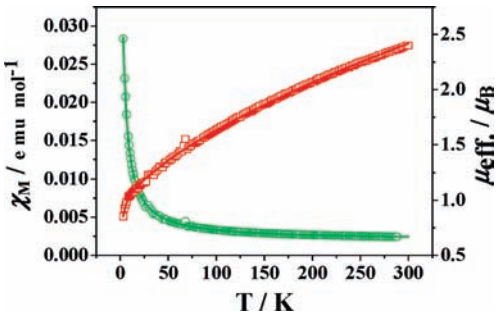

Figure 5. Variable-temperature magnetic susceptibility (○, green) and magnetic moment (□, red) under a magnetic field of 5 T of complex **2**.

Thus, **2** shows a complex response to the magnetic field displaying ferro- and antiferromagnetism. In addition, the antiferromagnetic interaction has both intra- and intermolecular components.

The nonlinear response of the magnetization toward the applied magnetic field prevents the use of any approximation to fit the experimental data. Since the weak ferromagnetism is repressed at high magnetic fields,[20] the fitting of the magnetic data at 5 T could therefore permit an approximation of the magnitude of antiferromagnetic interactions. The applied model[18,21] (eqs 1 and 2) considers a three-spin $S = 1/2$ system, with an intramolecular interaction between the ruthenium central atom and the two iminosemiquinone ligands (J_{Ru-Q}) together with an intramolecular interaction between the iminosemiquinone systems (J_{Q-Q}). In addition, we have also considered a weak intermolecular contact in the molecular field approximation and a TIP term.

$$\chi_M = \frac{Ng^2\beta^2\left[1+\exp\left(\frac{J_{Ru-Q}-J_{Q-Q}}{kT}\right)+10\exp\left(\frac{3J_{Q-Q}}{kT}\right)\right]}{3kT\left[1+\exp\left(\frac{J_{Ru-Q}-J_{Q-Q}}{kT}\right)+2\exp\left(\frac{3J_{Q-Q}}{kT}\right)\right]} \quad (1)$$

$$\chi = \frac{\chi_M}{1-\frac{2J}{Ng^2\beta^2}} + \mathrm{TIP} \quad (2)$$

The use of this model leads to a good agreement between the experimental and calculated data (Figure 5) with several sets of parameters. In all fits, the parameters show the following tendencies: low values of g (near 1.2), high values for the intramolecular coupling constants J_{Ru-Q} (on the order of -10^3 cm^{-1}) and J_{Q-Q} (on the order of -10^2 cm^{-1}), and small intermolecular antiferromagnetic coupling (J of about -3 cm^{-1}).

It is known that ferromagnetic impurities even in low concentrations in paramagnetic complexes can seriously affect the magnetic susceptibility results.[22a] Thus, the presence of parts per million levels of ferromagnetic impurities could give a behavior similar to that observed for **2**. However, the contribution of the fractional ferromagnetic impurity to the total susceptibility can be corrected using a strong applied magnetic field.[22] In the present case, the fits carried out using the corrected experimental data with the magnetization value at saturation lead to unreasonable parameters. This suggests that the ferromagnetism is an intrinsic property of **2**.

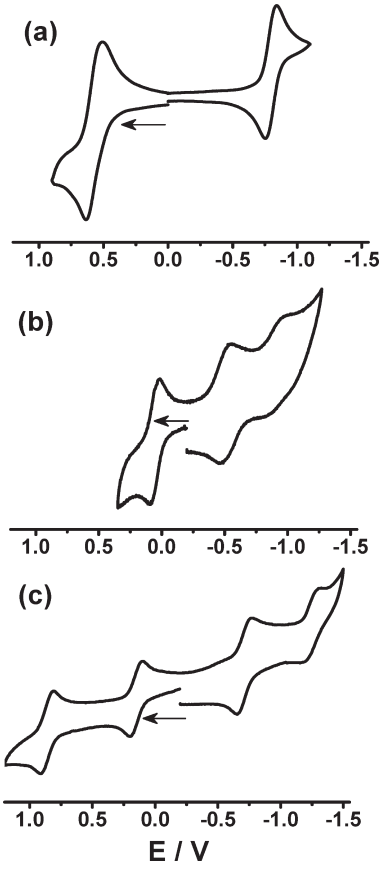

Figure 6. Cyclic voltammograms of (a) **1**, (b) **2**, and (c) **3** in CH_3CN/0.1 M $[Et_4N][ClO_4]$ versus SCE. Scan rate: 100 mV/s.

One has to consider the possibility of weak ferromagnetic coupling in **2**, in addition to the intra- and intermolecular antiferromagnetic interactions. The ferromagnetism can originate from uncompensated magnetic moments of the system, arising probably from a spin canting in all measured temperature ranges. Spin-canting is a well-known magnetic phenomenon in numerous inorganic compounds,[23] although it is unusual at room temperature in coordination complexes.

Therefore, **2** possesses a rather complicated magnetic behavior, including a strong dominant intramolecular antiferromagnetic coupling, an intermolecular antiferromagnetic interaction, and a weak ferromagnetic order. The high intramolecular antiferromagnetic interactions (J_{Ru-Q} and J_{Q-Q}) lead to one unpaired electron, as evident at low temperatures. In addition, an intermolecular antiferromagnetic interaction results in a magnetic moment lower than

(20) (a) Sweet, L. E.; Hughbanks, T. *Inorg. Chem.* **2006**, *45*, 9696. (b) Benbow, E. M.; Dalal, N. S.; Latturner, S. E. *J. Am. Chem. Soc.* **2009**, *131*, 3349.

(21) Mijangos, E.; Sánchez-Costa, J.; Roubeau, O.; Teat, S. J.; Gamez, P.; Reedijk, J.; Gasque, L. *Cryst. Growth Des.* **2008**, *8*, 3187.

(22) (a) Hatscher, S.; Schilder, H.; Lueken, H.; Urland, W. *Pure Appl. Chem.* **2005**, 77 497. (b) Boubekri, R.; Beji, Z.; Elkabous, K.; Herbest, F.; Viau, G.; Ammar, S.; Fiévet, F.; von Bardeleben, H. J.; Mauger, A. *Chem. Mater.* **2009**, *21*, 843.

(23) (a) Kahn, O. *Molecular Magnetism*; VCH Publishers: New York, 1993; p 321.(b) Yee, G. T.; Whitton, M. J.; Sommer, R. D.; Frommen, C. M.; Reiff, W. M. *Inorg. Chem.* **2000**, *39*, 1874. (c) Gao, E. Q.; Cheng, A. L.; Xu, Y. X.; He, M. Y.; Yan, C. H. *Inorg. Chem.* **2005**, *44*, 8822. (d) Wang, X. T.; Wang, Z. M.; Gao, S. *Inorg. Chem.* **2007**, *46*, 10452.

Table 4. Redox Potentials[a] and Comproportionation Constants for Complexes

compd	oxidation	reduction		K_{c1}[b]	K_{c2}[b]	K_{c3}[b]
1	0.56(80)	−0.80(80)			$10^{23.0}$	
2	0.07(70)	−0.49(100)	−0.87(150)		$10^{9.4}$	$10^{6.4}$
3	0.87(100) 0.16(100)	−0.69(100)	−1.23(100)	$10^{12.0}$	$10^{14.4}$	$10^{9.2}$
4	0.37(110)	−0.96(90)			$10^{22.5}$	
5[c]	1.67(110) 0.03(140)		−0.84(60)		$10^{27.7}$	$10^{14.7}$
6[d]	0.98(80)	−0.79(80)			$10^{30.0}$	

[a] Potentials $E_{298}°$ [V] (ΔE [mV]) versus SCE; in CH_3CN/0.1 M Et_4NClO_4 (for **1**−**4** and **6**) and in CH_2Cl_2/0.1 M Bu_4NPF_6 (for **5**); scan rate, 100 mV s^{-1}. [b] $RT \ln K_c = nF(\Delta E)$. K_{c1}, K_{c2}, and K_{c3} correspond to successive two oxidation processes, first oxidation and reduction processes, the first and second reduction processes, respectively. [c] Calculated from values versus ferrocenium/ferrocene (ref 6) by adding the empirical increment +0.45 V. [d] Reported potentials: 1.07 and −0.72 V by polarography with a rotating platinum electrode in DMF solvent versus SCE at 298 K (Seddon, E. A.; Seddon, K. R. *The Chemistry of Ruthenium*; Elsevier: Oxford, **1984**, 203).

one unpaired electron at 2 K. Finally, the weak ferromagnetism observed is tentatively attributed to spin-canting.

Electrochemical Oxidation and Reduction: Redox Potentials. The cyclic voltammograms of **1**−**3** are shown in Figure 6. The redox potentials and comproportionation constant values (K_c)[24] for the successive redox processes of **1**−**6** are set in Table 4. The results will be discussed after the individual electron transfer steps have been identified via spectroelectrochemical product identification.

EPR and UV−Vis−NIR Spectroelectrochemistry of the Redox System 1^m. Starting from EPR-silent **1** with the structurally suggested $Ru^{III}(Q^{\bullet-})$ oxidation state description, both the one-electron oxidation and one-electron reduction produce species $\mathbf{1}^+$ and $\mathbf{1}^-$, respectively, with ligand-based spin. The EPR spectra (Figure S11, Supporting Information) with g_{iso} close to the free electron value of $g = 2.0023$ are observable at room temperature and partially resolved. The similarity of the spectra (Figure S11) is remarkable. The available parameters for $\mathbf{1}^-$ ($\mathbf{1}^+$) are g_{iso} = 2.0034 (2.0036), $a(^1H)$ = 0.08 and 0.28 (0.15, 0.32) mT, $a(^{14}N)$ = 0.70 (0.75 mT), and total spectral width = 3.1 (3.3) mT. Due to restricted rotation around the N−C(phenyl) bond,[25] seven different C−H coupling constants are expected, of which only two could be identified at the outer sections of the EPR spectra, the remaining extensive hyperfine structure being only partially resolved. The N-aryl rings receive considerable spin density, as demonstrated also through the strong effect of aryl substitution at the site of electron transfer (mixed for the unsubstituted system **4**^{n},[8,26] metal-based in the present case **1**^{m}). The ^{14}N coupling is typical for *o*-iminobenzosemiquinones.[6,27] The anion $[Ru(Q)(acac)_2]^-$ shows $^{99,101}Ru$ satellite coupling (I = 5/2, 12.7%, and 17.0% natural abundance) of about 0.1 mT (Figure S11). The cation[6] $[Ru^{II}(Q^{\bullet-})(bpy)_2]^+$ (**5**$^+$, $a(^{14}N)$ = 0.78 mT) which is related to the anion $[Ru^{II}(Q^{\bullet-})(acac)_2]^-$ shows a much larger metal coupling of 1.01 mT (^{99}Ru) and 1.13 mT (^{101}Ru) at a higher g value of 2.0049, all of which signifies more pronounced metal contributions to the singly occupied molecular orbital in $\mathbf{5}^+$ relative to $\mathbf{1}^-$.

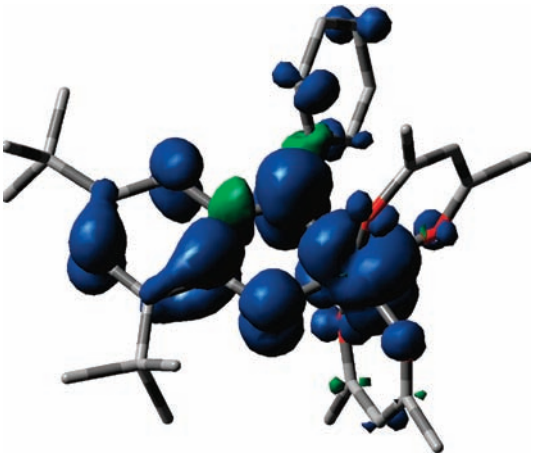

Figure 7. Spin density plot of $\mathbf{1}^-$.

Chart 1[a]

$\mathbf{1}^+$: $\mathbf{[Ru^{IV}(Q^{\bullet-})(acac)_2]^+}$ or $[Ru^{III}(Q^{o})(acac)_2]^+$

$\mathbf{1}^o$: $\mathbf{[Ru^{III}(Q^{\bullet-})(acac)_2]^o}$ or $[Ru^{II}(Q^{o})(acac)_2]^o$

$\mathbf{1}^-$: $[Ru^{III}(Q^{2-})(acac)_2]^-$ or $\mathbf{[Ru^{II}(Q^{\bullet-})(acac)_2]^-}$

[a] Preferred valence combination in boldface.

The DFT calculations on geometry-optimized **1** also predict that the highest occupied molecular orbital (HOMO) is predominantly a metal-based orbital with relative contributions of 57%, 17%, and 26% for Ru, Q, and acac, respectively (Table S3 and Figure S12, Supporting Information), the metal-based oxidation leaving the unpaired spin on $Q^{\bullet-}$ in $\mathbf{1}^+$ (Mulliken spin density distribution: 0.741, 0.184, and 0.073 for Q, Ru, and acac, respectively, Figure S13 and Table S4, Supporting Information). On the other hand, the lowest unoccupied molecular orbital (LUMO) of **1** is dominated by Q-based orbitals with relative contributions from the metal, Q, and acac at 31%, 63%, and 6%, respectively (Table S3). Accordingly, the singly occupied molecular orbital (SOMO) of $\mathbf{1}^-$ is mainly composed by Q (73%) along with a minor metal contribution of 22% (Table S5, Supporting Information); that is, the preferential reduction of ruthenium leaves most spin on $Q^{\bullet-}$ (Mulliken spin density distribution: 0.691, 0.282, and 0.019 for Q, Ru, and acac, respectively, Figure 7).

Alternative assignments (Chart 1) with ruthenium-centered spin would be expected to exhibit widely spread **g** tensor components because of the large spin−orbit coupling constant of ruthenium(III) and can therefore be ruled out.[6]

Both resulting species $[Ru^{IV}(Q^{\bullet-})(acac)_2]^+$ and $[Ru^{II}(Q^{\bullet-})(acac)_2]^-$ have thus been obtained from **1** through metal-centered electron transfer (Chart 1). This result differs from the one observed[8] and subsequently analyzed in great detail[26] for the N-unsubstituted system **4**^{n} where oxidation and reduction lead to significantly mixed metal/ligand spin distributions.[8,26] The aryl substitution at N appears to strongly enhance the stability of

(24) Creutz, C. *Prog. Inorg. Chem.* **1983**, *30*, 1.
(25) Stahl, T.; Kasack, V.; Kaim, W. *J. Chem. Soc., Perkin Trans. 2* **1995**, 2127.
(26) Remenyi, C.; Kaupp, M. *J. Am. Chem. Soc.* **2005**, *127*, 11399.
(27) (a) Stegmann, H. B.; Ulmschneider, K. B.; Hieke, K.; Scheffler, K. *J. Organomet. Chem.* **1976**, *118*, 259. (b) Burghaus, O.; Plato, M.; Rohrer, M.; Moebius, K.; MacMillan, F.; Lubitz, W. *J. Phys. Chem.* **1993**, *97*, 7639.

Table 5. UV−vis−NIR Data for $\mathbf{1}^m$, $\mathbf{2}^m$, and $\mathbf{3}^m$ in Various Oxidation States from OTTLE Spectroelectrochemistry[a]

compd	λ [nm] (ε [M^{-1} cm^{-1}])
$\mathbf{1}^+$	733sh, 603(17400), 550sh, 430(9900), 297sh, 265(20500), 237(25900)
1	538(13100), 428sh, 355(8500), 315sh, 271(22700), 238(21100)
$\mathbf{1}^-$	765(9100), 444(7100), 377(8300), 332(10700), 273(24100), 239(24800)
$\mathbf{2}^+$	900br, 654(10400), 433(2900), 270sh, 218(21200)
2	662(5700), 378sh, 270(8500), 220(21300)
$\mathbf{2}^-$	1200br, 851(3800), 523(1900), 330(5200), 265(9900), 219(20100)
$\mathbf{2}^{2-}$	708(1800), 535sh, 445(2600), 325sh, 262(11000), 220(17200)
$\mathbf{3}^{2+}$	502 (sh), 584 (23000), 770 (14500),
$\mathbf{3}^+$	437 (9900), 604 (22400), 837 (7300), 925 (6900), > 2000
3	332 (14100), 553 (15600), 725 (9600), 1278 (5500)
$\mathbf{3}^-$	490 (7200), 567 (6400), 817 (17400), 1000sh

[a] $\mathbf{1}^m$ and $\mathbf{2}^m$ in CH_3CN/0.1 M Bu_4NPF_6 and $\mathbf{3}^m$ in CH_2Cl_2/0.1 M Bu_4NPF_6

the iminosemiquinone ligand, shifting the electron transfer activity to the metal in a sensitive metal/noninnocent ligand situation.

In agreement with this interpretation, the unexpected spectral similarity between the iminosemiquinone complexes $\mathbf{1}^-$ and $\mathbf{1}^+$ in spite of the different oxidation states and d-electron configurations of the metals confirms rather weak π interaction of both $\{(acac)_2Ru^{II}\}$ and $[(acac)_2Ru^{IV}]^{2+}$ with the radical intermediate state $Q^{\bullet-}$ of the noninnocent ligand.

The assignments from Chart 1 correlate with the redox potentials from Table 4. The moderate differences between the redox systems $\mathbf{1}^m$ and $\mathbf{4}^n$ reflect the acceptor character of the N-phenyl substituent in $\mathbf{1}^m$. Nevertheless, the ca. 0.20 V difference is accompanied by a notable change in electron transfer character, metal-based for system $\mathbf{1}^m$ but mixed for system $\mathbf{4}^n$.[8,26] The comparison between $\mathbf{1}^m$ and $\mathbf{6}^n$ reveals a higher degree of covalency of the Ru^{IV} state for the former, the latter all-acac compound **6** having a higher oxidation potential. The comparison $\mathbf{1}^m$ versus $\mathbf{5}^k$ reflects the charge difference, which results in an anodic shift by about 1 V for the more positively charged bpy analog. The comproportionation constants of 10^{23} to 10^{30} are broadly comparable for the systems $\mathbf{1}^m$, $\mathbf{4}^n$, $\mathbf{5}^k$, and $\mathbf{6}^n$.

UV−vis−NIR spectroelectrochemistry is a valuable complement of the EPR method. The lowest-energy intense band in complex **1** appears at 538 nm (Figure S14, Supporting Information, and Table 5). TD-DFT calculations on **1** predict two intense $d\pi(Ru) \rightarrow \pi^*(Q)$ absorptions at 546 and 522 nm, corresponding to HOMO−1 → LUMO and HOMO−2 → LUMO transitions, respectively (Table S6, Supporting Information). The oxidation of **1** to $\mathbf{1}^+$ results in a bathochromic shift (538 → 603 nm) of the intense long-wavelength band (Figure S14, Table 5), interpreted as a mixed ligand-to-metal charge transfer/metal-to-ligand charge transfer (LMCT/MLCT) transition in **1** and as predominantly LMCT (iminosemiquinone → ruthenium(IV)) in $\mathbf{1}^+$. Conversely, the similarly shifted (538 → 765 nm) absorption for $\mathbf{1}^-$ is attributed to a ruthenium(II) → iminosemiquinone MLCT transition.

In comparison to the species $[Ru(Q)(bpy)_2]^+$ ($\mathbf{5}^+$)[6] with acceptor instead of donor coligands, the present example $\mathbf{1}^m$ shows the following: Among the pairs $[Ru^{II}(Q^{\bullet-})(acac)_2]^-$ ($\mathbf{1}^-$)/$[Ru^{II}(Q^{\bullet-})(bpy)_2]^+$ ($\mathbf{5}^+$) and $[Ru^{III}(Q^{\bullet-})(acac)_2]$ (**1**)/$[Ru^{III}(Q^{\bullet-})(bpy)_2]^{2+}$ ($\mathbf{5}^{2+}$), there is a great similarity of the absorption spectral data (Table 5), which justifies the assignments given. While the spectroelectrochemically obtained[6] $[Ru^{II}(Q^{2-})(bpy)_2]^o$ has no stable counterpart in the $Ru(acac)_2$ series, the $[Ru^{III}(Q^o)(bpy)_2]^{3+}$ ($\mathbf{5}^{3+}$) state[6] differs spectroscopically from the EPR-spectroscopically confirmed species $[Ru^{IV}(Q^{\bullet-})(acac)_2]^+$ ($\mathbf{1}^+$) as described here; in contrast to the neutral acceptor bpy, the $acac^-$ donor ligands have the ability to stabilize ruthenium in the +IV oxidation state.[28]

Chart 2

$\mathbf{2}^+$: $\mathbf{[Ru^{IV}(Q^{\bullet-})_2(acac)]^+}$ or $[Ru^{III}(Q^{\bullet-})(Q^o)(acac)]^+$

$\mathbf{2}^o$: $[Ru^{IV}(Q^{\bullet-})(Q^{2-})(acac)]^o$ or $\mathbf{[Ru^{III}(Q^{\bullet-})_2(acac)]^o}$ or $[Ru^{II}(Q^{\bullet-})(Q^o)(acac)]^o$

$\mathbf{2}^-$: $[Ru^{III}(Q^{\bullet-})(Q^{2-})(acac)]^-$ or $\mathbf{[Ru^{II}(Q^{\bullet-})_2(acac)]^-}$

$\mathbf{2}^{2-}$: $[Ru^{III}(Q^{2-})_2(acac)]^{2-}$ or $\mathbf{[Ru^{II}(Q^{\bullet-})(Q^{2-})(acac)]^{2-}}$

EPR and UV−Vis−NIR Spectroelectrochemistry of the Redox System $\mathbf{2}^m$. Anodic oxidation of **2** leads to the even-electron species $\mathbf{2}^+$ with the valence alternatives as delineated in Chart 2. The mixed LMCT/MLCT transition (iminosemiquinone/ruthenium(III)) gains in intensity but shows hardly any shift (Figure S15, Supporting Information, Table 5). In the visible region, complex **2** exhibits one moderately intense absorption at 662 nm (Table 5), and the TD-DFT calculations on **2** predict two close-lying transitions, $d\pi(Ru)/\pi(Q) \rightarrow \pi^*(Q)$, at 746 and 660 nm corresponding to HOMO−2(α) → LUMO(α)/HOMO−1(β) → LUMO(β) and HOMO−2(α) → LUMO(α)/HOMO−1(β)→ LUMO+1(β), respectively (Table S7, Supporting Information).

One-electron reduction to $\mathbf{2}^-$ causes a larger bathochromic shift (662 → 851 nm, Figure S15, Supporting Information), and the transition can be interpreted as MLCT/LLCT (Ru^{II}/acac → $Q^{\bullet-}$) in a $[Ru^{II}(Q^{\bullet-})_2(acac)]^-$ formulation. On the basis of the results for the second reduction, we prefer this oxidation state assignment. After the addition of a second electron, the resulting EPR signal at g_{iso} = 2.0046 (^{99,101}Ru coupling of 0.4 mT) points to ligand-based spin for $\mathbf{2}^{2-}$, compatible with $[Ru^{II}(Q^{\bullet-})(Q^{2-})(acac)]^{2-}$ but not with $[Ru^{III}(Q^{2-})^2$-$(acac)]^{2-}$. The long-wavelength band diminishes, and a weaker absorption remains at 708 nm. The intensity reduction can be attributed to a MLCT situation in $[Ru^{II}(Q^{\bullet-})(Q^{2-})(acac)]^{2-}$ whereby the one remaining iminosemiquinone acts as π acceptor for $d\pi(Ru^{II})$. Rather small redox potential differences and corresponding comproportionation constants (Table 4) reflect the increased number of redox-active components.

(28) (a) Maji, S.; Sarkar, B.; Mobin, S. M.; Fiedler, J.; Urbanos, F. A.; Aparicio, R. J.; Kaim, W.; Lahiri, G. K. *Inorg. Chem.* **2008**, *47*, 5204. (b) Kar, S.; Sarkar, B.; Ghumaan, S.; Roy, D.; Urbanos, F. A.; Fiedler, J.; Sunoj, R. B.; Jimenez-Aparicio, R.; Kaim, W.; Lahiri, G. K. *Inorg. Chem.* **2005**, *44*, 8715. (c) Hoshino, Y.; Higuchi, S.; Fiedler, J.; Su, C.-Y.; Knödler, A.; Schwederski, B.; Sarkar, B.; Hartmann, H.; Kaim, W. *Angew. Chem., Int. Ed.* **2003**, *42*, 674. (d) Ghumaan, S.; Sarkar, B.; Maji, S.; Puranik, V. G.; Fiedler, J.; Urbanos, F. A.; Jimenez-Aparicio, R.; Kaim, W.; Lahiri, G. K. *Chem.—Eur. J.* **2008**, *14*, 10816.

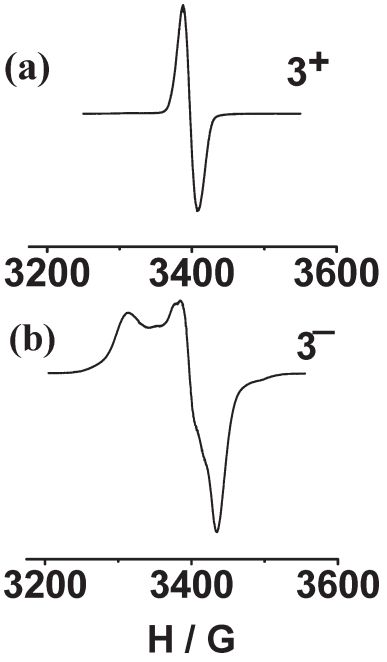

Figure 8. EPR spectra of (a) $\mathbf{3}^{+}$ and (b) $\mathbf{3}^{-}$ in CH_2Cl_2/Bu_4NPF_6 at 110 K.

EPR, UV−Vis−NIR Spectroelectrochemistry and TD-DFT Analysis of the Redox System $\mathbf{3}^{m}$. On the basis of arguments summarized by Pierpont and co-workers for related tris-chelate complexes,[3b] we attribute the imino-semiquinone oxidation state to all three ligands in neutral, EPR-silent **3**. This formulation is authenticated by the relevant bond distances in the crystal structure of **3** (Figure 2, Table 3, see above) and by the bond distances obtained for the DFT geometry-optimized structure of **3** (Figure S16, Supporting Information, Table 3). On one-electron oxidation to the intermediate $\mathbf{3}^{+}$, an intense unresolved EPR signal (Figure 8a) without detectable g anisotropy at X band frequency was observed (g_{iso} = 1.9945), both at room temperature and at 110 K. The absence of noticeable g component splitting signifies a very small metal contribution to the spin distribution in $\mathbf{3}^{+}$, as supported by DFT calculations (Mulliken spin distributions: 0.808 for Q and 0.192 for Ru, Figure 9a). One-electron reduction to intermediate $\mathbf{3}^{-}$ yields an isotropic g of 2.0018, very close to the free electron value; however, in glassy frozen solution at 110 K, there is an appreciable g component splitting observable with g_1 = 2.0455, g_2 = 1.994, and g_3 = 1.973 (Figure 8b). These values establish a metal/ligand mixed spin intermediate $\mathbf{3}^{-}$, in agreement with DFT calculation results (Mulliken spin distributions: 0.693 for Q and 0.307 for Ru, Figure 9b).

The symmetry of system $\mathbf{3}^{m}$ and the presence of three equivalent highly noninnocent ligands[13,16] are responsible for extended absorption in the visible and near-infrared regions, as shown by the qualitative MO diagram of **3** (Figure 10). The starting compound **3** exhibits NIR absorption with a band maximum at 1278 nm in addition to several shoulders and a band at a 553 nm maximum (Figure 11 and Table 5). The TD-DFT calculations (Table S8, Supporting Information) also suggest one NIR band at 1289 nm corresponding to the HOMO → LUMO transition as well as an absorption at 561 nm corresponding to transitions HOMO−2 → LUMO/

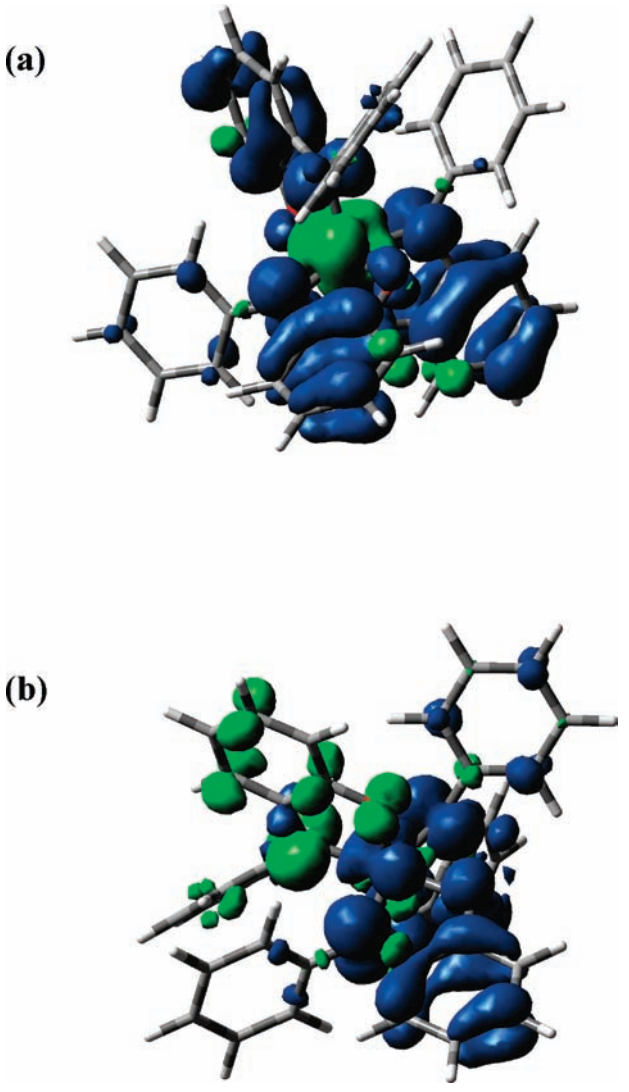

Figure 9. Spin densities for (a) $\mathbf{3}^{+}$ and (b) $\mathbf{3}^{-}$.

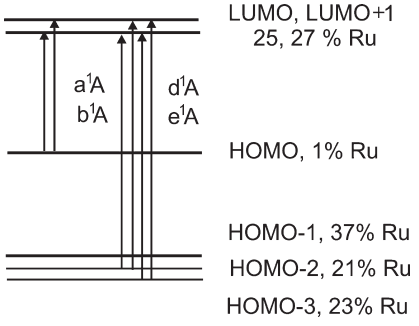

Figure 10. Qualitative MO scheme of **3**. Arrows indicate the main contributions to the lowest-allowed TD-DFT calculated transitions.

HOMO−3 → LUMO+1 (Table S8). Oxidation to $\mathbf{3}^{+}$ causes the NIR band to diminish while a very broad, weak band at > 2000 nm as well as absorption features at about 900 and 600 nm emerge (Figure 11). The latter remains hardly changed on a second oxidation, whereas the NIR band disappears and the 900 nm band system shifts to 770 nm (Figure 11). The TD-DFT calculations on $\mathbf{3}^{2+}$ also predict transitions in that region (Table S9, Supporting Information).

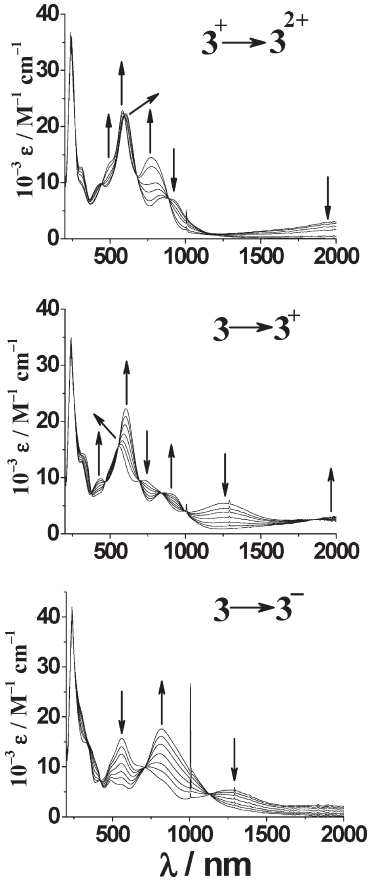

Figure 11. OTTLE spectroelectrochemistry for $\mathbf{3}^m$ in CH_2Cl_2/0.1 M Bu_4NPF_6. The peak at 1000 nm in the process of **3** to $\mathbf{3}^-$ conversion corresponds to a switching signal.

The very broad NIR absorption for $\mathbf{3}^+$ is not untypical for intervalence charge transfer transitions between coordinated but weakly interacting noninnocent ligands of different charges and oxidation states.[29] The formulation $[Ru^{III}(Q^{\bullet-})_2(Q^o)]^+$ from Chart 3 would provide such an opportunity (formally a semiquinone-to-quinone transition, SOMO → LUMO). For the doubly oxidized state, the HOMO is now empty, and no NIR transition can occur from this level. Intense charge transfer transitions involving the metal remain.

Reduction of **3** to $\mathbf{3}^-$ causes the long-wavelength NIR intensity to diminish while an intense feature at 817 nm absorption emerges. Due to the computationally and EPR-spectroscopically established metal/ligand orbital mixing, we attribute this band system to LMCT/MLCT mixed transitions, as also revealed from the MO diagram (Figure 10). After adding the second electron to form $\mathbf{3}^{2-}$, the absorption band just loses intensity, suggesting the main participation of the stepwise converted semiquinone in the transition. The redox potentials (Table 4) and moderately large comproportionation constants indicate considerable Coulombic interaction between the three ruthenium(III)-bound ligands.

Chart 3

$\mathbf{3}^{2+}$: $[Ru^{IV}(Q^{\bullet-})_2(Q^o)]^{2+}$ or $\mathbf{[Ru^{III}(Q^{\bullet-})(Q^o)_2]^{2+}}$

$\mathbf{3}^{+}$: $[Ru^{IV}(Q^{\bullet-})_3]^{+}$ or $\mathbf{[Ru^{III}(Q^{\bullet-})_2(Q^o)]^{+}}$

$\mathbf{3}^{o}$: $[Ru^{IV}(Q^{\bullet-})_2(Q^{2-})]^{o}$ or $\mathbf{[Ru^{III}(Q^{\bullet-})_3]^{o}}$ or $[Ru^{II}(Q^{\bullet-})_2(Q^o)]^{o}$

$\mathbf{3}^{-}$: $\mathbf{[Ru^{III}(Q^{\bullet-})_2(Q^{2-})]^{-}}$ or $[Ru^{II}(Q^{\bullet-})_3]^{-}$

$\mathbf{3}^{2-}$: $\mathbf{[Ru^{III}(Q^{\bullet-})(Q^{2-})_2]^{2-}}$ or $[Ru^{II}(Q^{\bullet-})_2(Q^{2-})]^{2-}$

Comparison and Conclusion. Using the pervasive[30] ruthenium complex framework with three bidentate chelate ligands in an approximately octahedral configuration, the successive replacement of the largely[9,10,17] innocent $acac^-$ standard by the highly noninnocent iminoquinonoid Q^m in systems **1**−**3** has been analyzed to produce a fascinating array of different electronic structures. Both the stability of the semiquinone radical ligand $Q^{\bullet-}$ and its two-sided electron transfer capacity have been noted in the three redox series which were analyzed especially via EPR and UV−vis−NIR spectroelectrochemistry. Within the $[Ru(Q)_n(acac)_{3-n}]^m$ series (n = 1, 2, 3), distinct differences in terms of involvement of metal- or Q-based redox orbitals on electron-transfer processes have been recognized. Pronounced participation of Q-based frontier orbitals at oxidation and reduction processes occurs with an increasing number of ligands Q in the complex. Moreover, the significant differences between N-phenyl-substituted $\mathbf{1}^m$ with metal-centered electron transfer and N-unsubstituted $\mathbf{4}^n$[8,26] with mixed metal/ligand involving electron transfer demonstrate a high sensitivity of the system and the potential of redox tuning. The other option, the variation of the more innocently behaving coligand from $acac^-$ to 2,2′-bipyridine, is also being illustrated through comparison between $\mathbf{1}^m$ and $\mathbf{5}^k$.[6]

Finally it is conspicuous that *all* favored oxidation state formulations from Charts 1−3, based on structural, magnetic, electrochemical, and spectroscopic characterization, exhibit the iminosemiquinone−ruthenium entity. This demonstration of the remarkable stability of that arrangement coincides with the use of this particular combination in challenging electron transfer processes such as water oxidation catalysis,[31] and it may be exploited further in the development of functional radical-containing systems.[32]

Experimental Section

Materials. The precursor complex $Ru(acac)_2(CH_3CN)_2$[33] and the ligand 2-anilino-4,6-di-*tert*-butylphenol(H_2Q)[34,19] were

(29) (a) Chakraborty, S.; Laye, R. H.; Paul, R. L.; Gonnade, R. G.; Puranik, V. G.; Ward, M. D.; Lahiri, G. K. *J. Chem. Soc., Dalton Trans.* **2002**, 1172. (b) Metcalfe, R. A.; Vasconcellos, L. C. G.; Mirza, H.; Franco, D. W.; Lever, A. B. P. *J. Chem. Soc., Dalton Trans.* **1999**, 2653. (c) Auburn, P. R.; Lever, A. B. P. *Inorg. Chem.* **1990**, *29*, 2551. (d) Ghumaan, S.; Mukherjee, S.; Kar, S.; Roy, D.; Mobin, S. M.; Sunoj, R. B.; Lahiri, G. K. *Eur. J. Inorg. Chem.* **2006**, 4426.

(30) Juris, A.; Balzani, V.; Barigelletti, F.; Campagna, S.; Belser, P.; von Zelewsky, A. *Coord. Chem. Rev.* **1988**, *84*, 85.

(31) (a) Muckerman, J. T.; Polyansky, D. E.; Wada, T.; Tanaka, K.; Fujita, E. *Inorg. Chem.* **2008**, *47*, 1787. (b) Wada, T.; Tsuge, K.; Tanaka, K. *Inorg. Chem.* **2001**, *40*, 329. (c) Wada, T.; Tsuge, K.; Tanaka, K. *Angew. Chem., Int. Ed.* **2000**, *39*, 1479. (d) Tsai, M. K.; Rochford, J.; Polyansky, D. E.; Wada, T.; Tanaka, K.; Fujita, E.; Muckerman, T. J. *Inorg. Chem.* **2009**, *48*, 4372.

(32) Jain, R.; Caldwell, S. L.; Louie, A. S.; Hicks, R. G. *Can. J. Chem.* **2006**, *84*, 1263.

(33) Kobayashi, T.; Nishina, Y.; Shimizu, K. G.; Satô, G. P. *Chem. Lett.* **1988**, 1137.

(34) (a) Maslovskaya, L. A.; Petrikevich, D. K.; Timonshchuk, V. A.; Shadyro, O. I. *Russ. J. Gen. Chem.* **1996**, *66*, 1842. Translated from: *Zh. Obsh. Khim.* **1996**, *66*, 1893. (b) FRG Patent No. 1 104522, **1959**. *Chem. Abstr.* **1962**, *56*, 5887.

prepared according to the reported procedures. Other chemicals and solvents were of reagent grade and used as received.

Instrumentation. UV−vis−NIR spectroelectrochemical studies were performed in CH_3CN/0.1 M Bu_4NPF_6 at 298 K using an optically transparent thin-layer electrode (OTTLE) cell[35] mounted in the sample compartment of a J&M TIDAS spectrophotometer. ^{1}H NMR spectra of **1** and **3** were obtained with 300 MHz Varian and 250 MHz Bruker FT spectrometers, respectively. The EPR measurements were made in a two-electrode capillary tube[36] with an X-band (9.5 GHz) Bruker system ESP300 spectrometer. The EPR measurements for **2** were made with a Varian model 109C E-line X-band spectrometer fitted with a quartz Dewar for 77 K. Cyclic voltammetric, differential pulse voltammetric, and coulometric measurements were carried out using a PAR model 273A electrochemistry system. Platinum wire working and auxiliary electrodes and an aqueous saturated calomel reference electrode (SCE) were used in a three-electrode configuration. The supporting electrolyte was 0.1 M Et_4NClO_4, and the solute concentration was ca. 10^{-3} M. The half-wave potential $E_{298}°$ was set equal to $0.5(E_{pa} + E_{pc})$, where E_{pa} and E_{pc} are anodic and cathodic cyclic voltammetric peak potentials, respectively. Elemental analyses were carried out with a Perkin-Elmer 240C elemental analyzer. Electrospray mass spectra were recorded on a Micromass Q-ToF mass spectrometer.

Crystallography. Single crystals of **1** and **3** were grown by slow evaporation of their 1:1 acetonitrile−hexane solutions at 298 K. X-ray diffraction data were collected using an OXFORD XCALIBUR-S CCD single-crystal X-ray diffractometer. The structures were solved and refined by full-matrix least-squares techniques on F^2 using the SHELX-97 program.[37] The absorption corrections were done using the multiscan technique. All data were corrected for Lorentz and polarization effects, and the non-hydrogen atoms were refined anisotropically. Hydrogen atoms were included in the refinement process as per the riding model.

Magnetic Measurements. The variable-temperature magnetic susceptibilities were measured on polycrystalline samples with a Quantum Design MPMSXL SQUID (Superconducting Quantum Interference Device) susceptometer over a temperature range of 2−300 K at the constant fields of 0.1, 1, and 5 T. Each raw data set was corrected for the diamagnetic contribution of both the sample holder and the complex to the susceptibility. The molar diamagnetic corrections were calculated on the basis of Pascal constants. Magnetization measurements were carried out at 2, 100, and 300 K from 0 to 5 T, including also hysteresis loops between −5 and +5 T at 2 and 300 K. The ZFC and FC susceptibility were measured in a magnetic field of 0.1 T from 2 to 300 K. The fitting of the experimental data was carried out using the MATLAB V.5.1.0.421 program.

DFT Calculations. Full geometry optimizations were carried out using the density functional theory method at the (R)B3LYP level for **1** and **2** and the (U)B3LYP level for $\mathbf{1}^+$ and $\mathbf{1}^-$.[38] All elements except ruthenium were assigned the 6-31G(d) polarized double-ζ basis set.[39] The effective core pseudopotentials and corresponding optimized sets were employed for the ruthenium atom.[40] The vibrational frequency calculations were performed to ensure that the optimized geometries represent the local minima and there are only positive eigenvalues. All calculations were performed with the Gaussian 03 program package.[41] Vertical electronic excitations based on optimized geometries were computed using the TD-DFT formalism[42] in acetonitrile, using the conductor-like polarizable continuum model.[43] The electronic structure of complex **3** was calculated by using the Perdew, Burke, and Ernzerhof[44] (PBE0) hybrid density functional.

Synthesis of [Ru(acac)$_2$(Q)] (1) and [Ru(acac)(Q)$_2$] (2). The precursor complex [Ru(acac)$_2$ (CH_3CN)$_2$] (50 mg, 0.13 mmol), 2-anilino-4,6-di-*tert*-butylphenol (H_2L) (96.5 mg, 0.33 mmol), and sodium acetate (53.3 mg, 0.65 mmol) were mixed in 20 mL of ethanol, and the mixture was heated to reflux for 24 h under atmospheric conditions. The initial orange red color changed to purple. The solvent of the reaction mixture was evaporated to dryness under reduced pressure. It was then purified on a silica gel column. The purple product corresponding to **1** was eluted with CH_2Cl_2, followed by the blue product (**2**) being eluted with acetonitrile−methanol (1:1). Evaporation of the solvent under reduced pressure afforded the pure complexes.

Complex **1**. Yield: 48 mg (61%). Anal. Calcd (Found) $C_{30}H_{39}O_5NRu$: C, 60.49 (60.63); H, 6.60 (6.77); N 2.35 (2.27). ESI MS (in CH_3CN) Calcd (Found) for $[\mathbf{1}]^+$: m/z 595.19 (596.35). ^{1}H NMR in $CDCl_3$ (δ, ppm(J, Hz)): 7.39(1H), 7.33(3H), 7.24(2H), 7.13(1H), 5.62(s, 1H), 5.14(s, 1H), 2.62(s, 3H), 2.00(s, 3H), 1.99(s, 3H), 1.82(s, 3H), 1.56(s, 9H), 1.45(s, 9H).

Complex **2**. Yield: 25 mg (24%). Anal. Calcd (Found) $C_{45}H_{57}O_4N_2Ru$: C, 68.24 (68.18); H, 7.26 (7.81); N 3.54 (3.43). ESI MS (in CH_3CN) Calcd (Found) for $[\mathbf{2}]^+$: m/z 791.33 (791.52).

Synthesis of [Ru(Q)$_3$] (3). $RuCl_3 \cdot 3H_2O$ (100 mg, 0.48 mmol), the ligand 2-anilino-4,6-di-*tert*-butylphenol (H_2Q, 570 mg, 1.92 mmol), and KOH (215 mg, 3.84 mmol) were taken in 30 mL methanol. The solution was stirred for 24 h at room temperature. The initial dark-brown-colored solution changed to a deep blue. The solvent was then removed under reduced pressure. The solid dry mass was dissolved in a minimum volume of (5−7 mL) dichloromethane, and the solution was filtered. The filtrate was collected, and the solvent was removed under reduced pressure. The dried product was then subjected to column chromatography on an alumina (neutral) column. The deep blue solution corresponding to **3** was eluted with CH_2Cl_2. Evaporation of the solvent under reduced pressure afforded the pure complex **3**.

Yield: 285 mg (60%). Anal. Calcd (Found) $C_{60}H_{75}N_3O_3Ru$: C, 72.99 (73.03); H, 7.66 (7.66); N, 4.26 (3.96). ESI MS (in CH_2Cl_2) Calcd (Found) for $[\mathbf{3}]^+$: m/z 987.48 (987.47). ^{1}H NMR in $CDCl_3$ (δ, ppm): 5.95 (s, 2H), 6.36 (s, 2 H), 6.55 (s, 2H), 6.87 (m, 5H), 7.03 (m, 5H), 7.15 (m, 5H), 0.91 (s, 9H), 0.98 (s, 9H), 1.11 (s, 9H), 1.21−1.15 (m, 27H).

Acknowledgment. Financial support received from the Department of Science and Technology and University Grant commission (New Delhi, India); from the DAAD and the DFG (Germany, Mercator Guest Professorship of G.K.L.); the Spanish MICINN, CM, and UCM-BSCH (projects no. CTQ2008-00920, S-0505-MAT-0303, and UCM-921073-4120824); and the grant agency of the Academy of Sciences of

(35) Krejcik, M.; Danek, M.; Hartl, F. *J. Electroanal. Chem.* **1991**, *317*, 179.
(36) Kaim, W.; Ernst, S.; Kasack, V. *J. Am. Chem. Soc.* **1990**, *112*, 173.
(37) Sheldrick, G. M. *SHELXS97*; University of Göttingen: Göttingen, Germany, 1997.
(38) Lee, C.; Yang, W.; Parr, R. G. *Phys. Rev. B* **1988**, *37*, 785.
(39) Hariharan, P. C.; Pople, J. A. *Theor. Chim. Acta* **1973**, *28*, 213.
(40) (a) Andrae, D.; Haeussermann, U.; Dolg, M.; Stoll, H.; Preuss, H. *Theor. Chim. Acta* **1990**, *77*, 123. (b) Fuentealba, P.; Preuss, H.; Stoll, H.; Szentpaly, L. V. *Chem. Phys. Lett.* **1989**, *89*, 418.
(41) Frisch, M. J. et al. *Gaussian 03*; Gaussian, Inc.: Wallingford, CT, 2004.
(42) (a) Bauernschmitt, R.; Ahlrichs, R. *Chem. Phys. Lett.* **1996**, *256*, 454. (b) Stratmann, R. E.; Scuseria, G. E.; Frisch, M. J. *J. Chem. Phys.* **1998**, *109*, 8218. (c) Casida, M. E.; Jamorski, C.; Casida, K. C.; Salahub, D. R. *J. Chem. Phys.* **1998**, *108*, 4439.
(43) (a) Barone, V.; Cossi, M. *J. Phys. Chem. A* **1998**, *102*, 1995. (b) Cossi, M.; Barone, V. *J. Chem. Phys.* **2001**, *115*, 4708. (c) Cossi, M.; Rega, N.; Scalmani, G.; Barone, V. *J. Comput. Chem.* **2003**, *24*, 669.
(44) (a) Perdew, J. P.; Burke, K.; Ernzerhof, M. *Phys. Rev. Lett.* **1996**, *77*, 3865. (b) Adamo, C.; Barone, V. *J. Chem. Phys.* **1999**, *110*, 6158.

the Czech Republic (S.Z., grant KAN100400702) is gratefully acknowledged. X-ray structural studies for **1** and **3** were carried out at the National Single Crystal Diffractometer Facility, Indian Institute Technology Bombay. ^{1}H NMR spectroscopy of **1** and EPR of **2** were carried out at the Sophisticated Analytical Instrument Facility (SAIF), Indian Institute Technology Bombay.

Supporting Information Available: X-ray crystallographic files in CIF format for **1** and **3**; DFT data set for **1** (Figures S12, S13), **2** (Figures S1, S2), and **3** (Figure S16); magnetic data for **2** (Figures S3−S10); EPR spectra of $\mathbf{1}^{m}$ (Figure S11); and spectroelectrochemistry figures for $\mathbf{1}^{m}$ (Figure S14) and $\mathbf{2}^{m}$ (Figure S15). This material is available free of charge via the Internet at http://pubs.acs.org.